THE JOURNAL OF PHYSICAL CHEMISTRY LETTERS
A JOURNAL OF THE AMERICAN CHEMICAL SOCIETY

pubs.acs.org/JPCL Letter

Ionization-Induced Double Charge Transfer in Metallophthalocyanines Revealed by *Ab Initio* Simulation of 2p Photoelectron Spectra

S. Carniato, R. Püttner, M. Briant, E. Gloaguen, K. Marmorat, M. Labeye, P. Çarçabal, and G. Goldsztejn*

Cite This: *J. Phys. Chem. Lett.* 2026, 17, 4804−4810 Read Online

ACCESS | Metrics & More | Article Recommendations | Supporting Information

ABSTRACT: We report on a joint experimental and theoretical investigation of the metal 2p X-ray photoelectron spectra of transition-metal phthalocyanines MnPc, FePc, and CoPc. Using a multiconfigurational approach including spin−orbit coupling, we obtain nearly quantitative agreement with experiment. In all investigated systems, we found an unexpected and robust physical effect induced by core ionization, namely a drastic reorganization of the valence electronic structure. This reorganization is characterized by a pronounced stabilization of doubly excited ligand-to-metal charge-transfer configurations, which become energetically favored in the final states. This ionization-induced double charge transfer is found to be common to all metallophthalocyanines studied. Furthermore, we identify a nearly linear correlation between the stabilization energies obtained from restricted active space configuration interaction (RAS-CI) calculations and a simple hydrogenic/Slater screening estimate, providing an intuitive and practical descriptor to assess when such charge-transfer states are expected to dominate after core ionization.

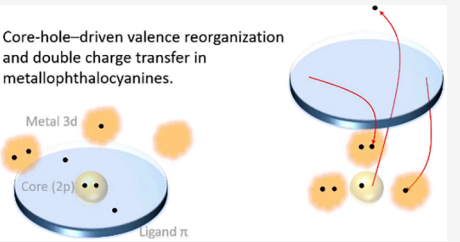

Metallophthalocyanines (MPc) are synthetic tetrapyrrolic molecules (see Figure 1) that have attracted a significant amount of interest because of their possible applications in a wealth of domains such as optoelectronics,[1] spintronics,[2] catalysis,[3] and photodynamic therapy.[4] Compared to their closely related natural molecular counterparts, the metalloporphyrins, the carbon atoms of the methine bridge are replaced by nitrogen atoms. This replacement has an influence on the metal−nitrogen distances and, therefore, the hybridization of the orbitals of the ligands as well as the metal−ligand interactions of these molecules.

A significant part of the studies on MPc molecules focuses on the characterization of their electronic ground state, i.e., the identification of the electron configurations formed by the 3d orbitals of the metal center and the resulting spin states. Interestingly, there is much controversy about both of these issues as we discussed for FePc,[5] where we have developed a strategy to characterize the ground state using photoelectron spectra measured for different shells. Indeed, MnPc, FePc, and CoPc share one peculiarity, namely, that the energy of the $3d_{x^2-y^2}$ (b_{1g} symmetry) orbital is too high for it to be populated in the ground state. Thus, these molecules can be considered as being in a frustrated high-spin situation that results in intermediate spin states. However, the ordering of the 3d orbitals can be identified more or less clearly depending on the theoretical or experimental method used. The same holds for the interpretation of experimental spectra where various spin states and even mixed-spin descriptions[6] have been proposed.

While numerous X-ray absorption spectroscopy (XAS) studies have been performed and the corresponding spectra simulated using DFT/ROCIS, charge-transfer multiplet (CTM), or multireference *ab initio* methods,[7−14] only a few X-ray emission spectroscopy (XPS) measurements have been reported, typically accompanied by CTM or DFT-CI simulations.[5,15] Compared to XAS that provides information about the core hole and the virtual orbitals, XPS allows direct probing of the core-ionized final states and is, therefore, particularly sensitive to relaxation and charge-transfer effects induced by the core hole.

From a theoretical perspective, the interpretation of core-level photoelectron spectra remains challenging, especially for transition-metal complexes with a pronounced multireference character. In this work, we use multiconfigurational *ab initio* simulations of metal 2p X-ray photoelectron spectra to investigate how core ionization affects the valence electronic structure of metallophthalocyanines. By combining experiment and theory for MnPc, FePc, and CoPc, we show that the creation of a 2p core hole induces a drastic reorganization of

Received: February 11, 2026
Revised: March 24, 2026
Accepted: March 25, 2026
Published: April 8, 2026

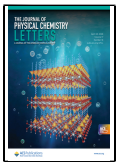

https://doi.org/10.1021/acs.jpclett.6c00486
J. Phys. Chem. Lett. 2026, 17, 4804−4810

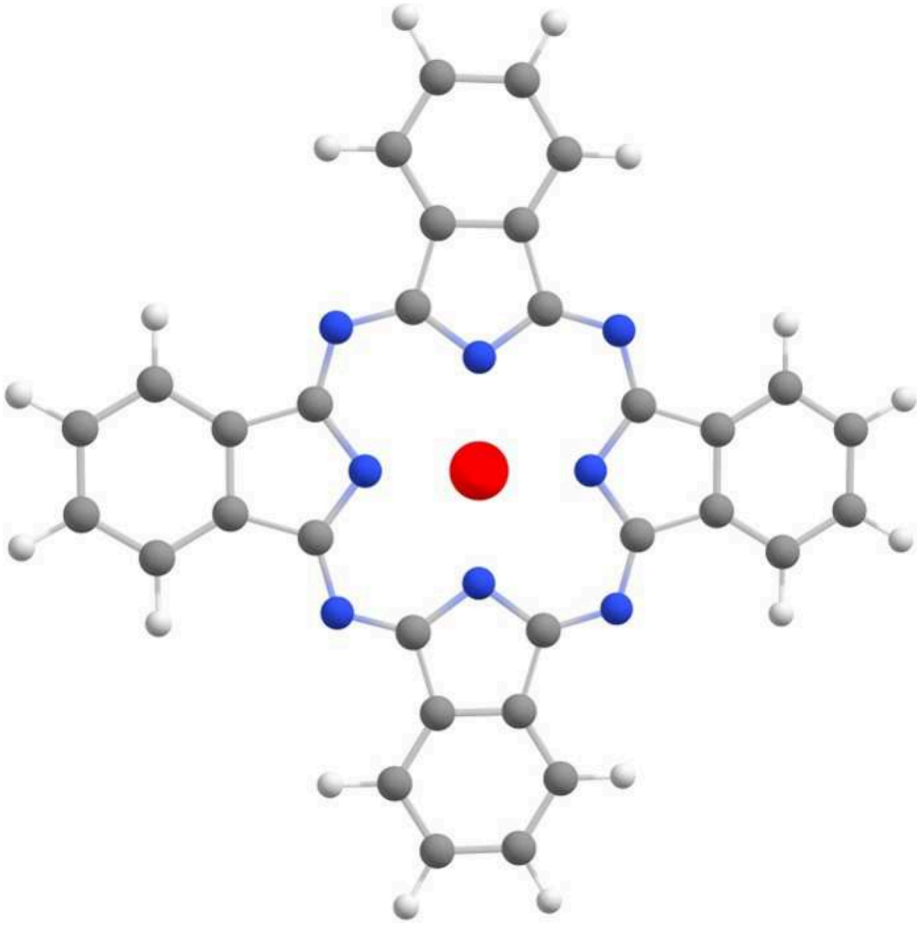

Figure 1. Representation of a metallophthalocyanine molecule. The red sphere in the center represents a dicationic metal atom (Mn^{2+}, Fe^{2+}, or Co^{2+} in this case), surrounded by doubly deprotonated phthalocyanine Pc^{2-}. The blue spheres represent the N atoms, the gray spheres the C atoms, and the white spheres the H atoms.

the valence electronic structure, characterized by the stabilization of doubly excited ligand-to-metal charge-transfer configurations, which become energetically favored in the final states. This unexpected ionization-induced double charge transfer is found to be a common feature of all MPc investigated here and provides new insight into the interpretation of transition-metal 2p XPS spectra.

The experiments have been performed at the French synchrotron facility SOLEIL using the PLEIADES beamline, which provides access to photon energies in the range of 10−1000 eV using an Apple II type of undulator. This range covers the 2p thresholds of the first period of transition metals (Ti−Cu) with binding energies (E_b) of ≈500−1000 eV. The photoelectron spectra were measured using a VG-Scienta R4000 hemispherical analyzer set at the magic angle (54.7° relative to the polarization direction of the synchrotron radiation) in order to avoid angular-distribution effects on the measured photoionization cross sections.[16]

In the present work, the molecules are measured in the gas phase. This approach has advantages and disadvantages as compared to measuring thin films. Thin films provide higher target densities leading to better statistics and allow for higher resolution. In contrast, gas-phase measurements exclude effects due to intermolecular interactions. To evaporate the molecules, we used a specifically custom-built oven inserted into the detection chamber. The molecules were evaporated at ≈700 K, leading to additional thermal broadening as compared to the spectra of thin films measured at room temperature. The pressure and temperature inside the chamber were controlled and monitored during data acquisition. All molecules have been purchased from Porphychem (purity of >95%) and further sublimated for purification. The 2p photoelectron spectra were recorded over a kinetic energy range of 40−50 eV using a step width of 0.25 eV and a total experimental resolution of ≈1.5 eV. The presented spectra were recorded over a time span of ≈2 h each.

Conceptually, XPS and X-ray emission spectroscopy (XES) are closely related processes. In detail, the 2p photoemission and 1s ← 2p X-ray emission probe the same manifold of $2p^{-1}$ core-ionized final states and differ primarily in the nature of the initial state and the associated dipole transition. In XPS, the transition involves the electronic ground state and a core-ionized final state accompanied by a continuum photoelectron, whereas XES corresponds to radiative transitions between a $1s^{-1}$ core-ionized intermediate state and the same set of $2p^{-1}$ final states.

From a computational perspective, the main challenge in simulating photoelectron spectra lies in the proper treatment of the emitted continuum electron, while for X-ray emission, the transition dipole matrix elements between bound many-electron states can be evaluated directly within standard multiconfigurational quantum-chemistry packages. This fact is the starting point of our approach, in which calculations for X-

https://doi.org/10.1021/acs.jpclett.6c00486
J. Phys. Chem. Lett. 2026, 17, 4804−4810

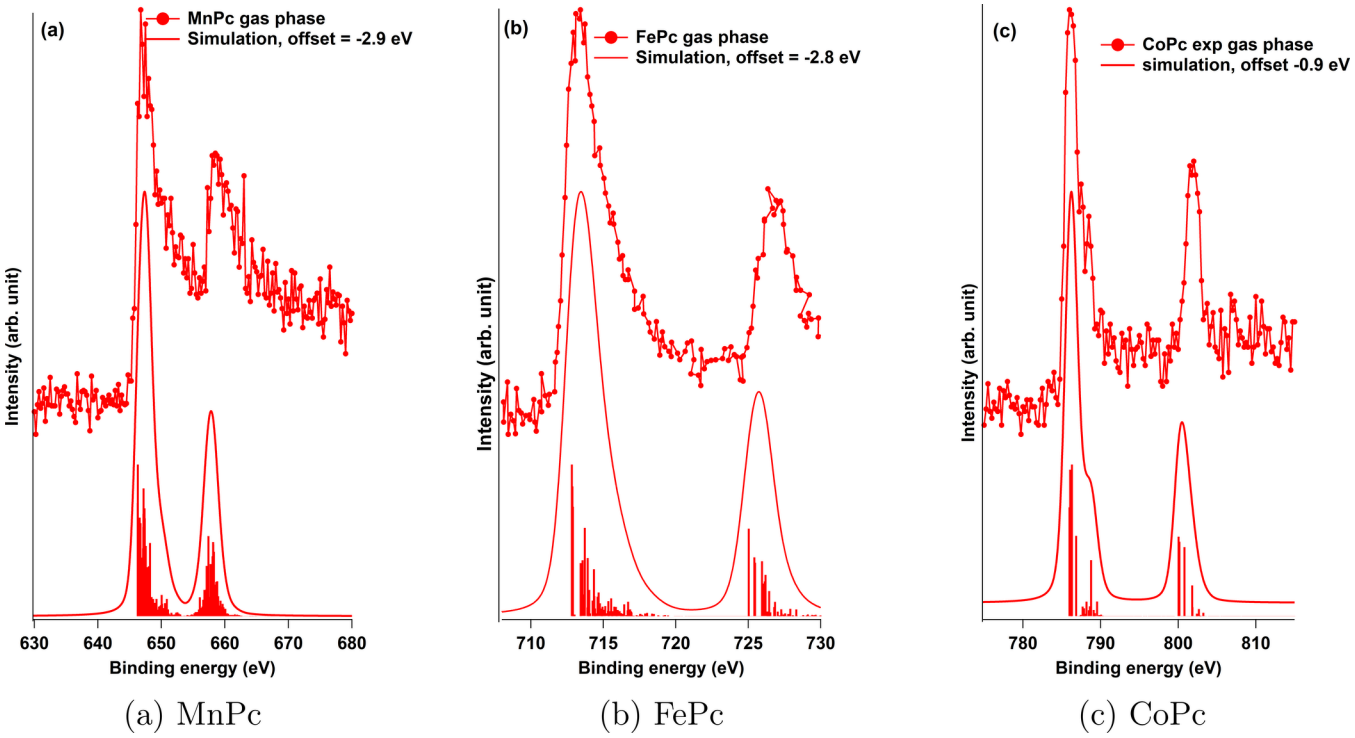

Figure 2. Experimental 2p photoelectron spectra of the MPc molecules (markers and top solid line), together with the simulated spectra (bottom solid line) and the individual intensities (sticks in the bottom part).

ray emission spectra are used to access the relative intensities of the $2p^{-1}$ final states observed in photoemission spectra.

In the following, we shall show how the intensities of core-level photoelectron and X-ray emission spectra can be related to each other. Within the one-step picture of photoemission, the intensities associated with a photoelectron of kinetic energy ϵ_k can be described with transition amplitudes between N-electron ground state $\Psi_0(N)$ and final states $\Psi^{\vec{k}}_{k,F}(N)$, which include a continuum photoelectron[15]

$$I_{XPS}(\epsilon_k, \hat{\mathbf{k}}) \propto |\langle \phi_k|\boldsymbol{\epsilon}\cdot\mathbf{r}|\phi_{2p}\rangle\langle \Psi_F(N-1)|\Psi_0^{(2p)}(N-1)\rangle|^2 \quad (1)$$

where ϕ_k is the continuum orbital of the emitted electron, $\boldsymbol{\epsilon}$ the polarization vector of the radiation, and $\Psi_0^{(2p)}(N-1)$ the normalized state obtained by annihilating a 2p electron from $\Psi_0(N)$ but without further relaxation. $\Psi_F(N-1)$ denotes the final $(N-1)$-electron state, describing the ionized system after photoemission. The full derivation of eq 1 is given in the Supporting Information.

In the case of X-ray emission spectroscopy (XES), starting from a $1s^{-1}$ intermediate state, the corresponding intensity reads

$$I_{XES} \propto |\langle \phi_{1s}|\boldsymbol{\epsilon}\cdot\mathbf{r}|\phi_{2p}\rangle\langle \Psi_F(N-1, 2p^{-1})|\Psi_0^{(1s)}(N-1)\rangle|^2 \quad (2)$$

where $\Psi_0^{(1s)}(N-1)$ is the normalized state obtained by annihilating a 1s electron from $\Psi_0(N)$. The full derivation of eq 2 is also given in the Supporting Information.

To compare intensities of X-ray photoelectron and X-ray emission spectra, two standard approximations are invoked. (i) Within the spectator approximation, the valence electrons do not significantly affect the one-electron dipole matrix element $\langle \phi_{1s}|\boldsymbol{\epsilon}\cdot\mathbf{r}|\phi_{2p}\rangle$ for the X-ray emission process. (ii) In the photoemission process, the variation of this dipole matrix element across the few-electronvolt $2p^{-1}$ multiplet manifold is negligible. With these assumptions, the intensity ratios of the different 1s ← 2p X-ray transitions become proportional to the $2p^{-1}$ photoelectron emissions, leading to the same final states. As a result, XES reflects the relative populations of the $2p^{-1}$ multiplet states observed in XPS. In practice, the XPS spectra were not obtained by this analogy, but by the direct evaluation of multiconfigurational dipole transition matrix elements as implemented in ORCA; eqs 1 and 2 are introduced to show the correspondence between X-ray photoelectron and emission spectroscopy.

In detail, the electronic structure calculations were performed following established multiconfigurational protocols previously applied to core-level spectroscopies.[17] Assuming that the metal center and its multiplet structure dominate the 2p XPS spectra, we first carried out state-averaged complete active space self-consistent field (SA-CASSCF) calculations for the ground state. The active space comprised predominantly metal-centered orbitals, namely, the five 3d orbitals and the highest occupied molecular orbital (HOMO) π_{Pc} of the ligand, as further discussed below.

Following the SA-CASSCF calculation, the metal 1s and 2p orbitals were rotated into the active space, and restricted active space configuration interaction (RAS-CI) calculations were performed for the $(N-1)$-electron ionized states, keeping the previously optimized orbitals frozen. In these state-averaged RAS-CI calculations, only single-ionization and double-excitation configurations were included in order to limit the number of states to a tractable size, typically fewer than 1000 states per spin multiplicity. As discussed by Pollock et al.,[17] the XES process predominantly involves the lowest-energy ionic state with a single 1s hole only but without further relaxation, which is a prerequisite for the applicability of the XES/XPS comparison outlined above. Accordingly, transitions were

https://doi.org/10.1021/acs.jpclett.6c00486
J. Phys. Chem. Lett. 2026, 17, 4804−4810

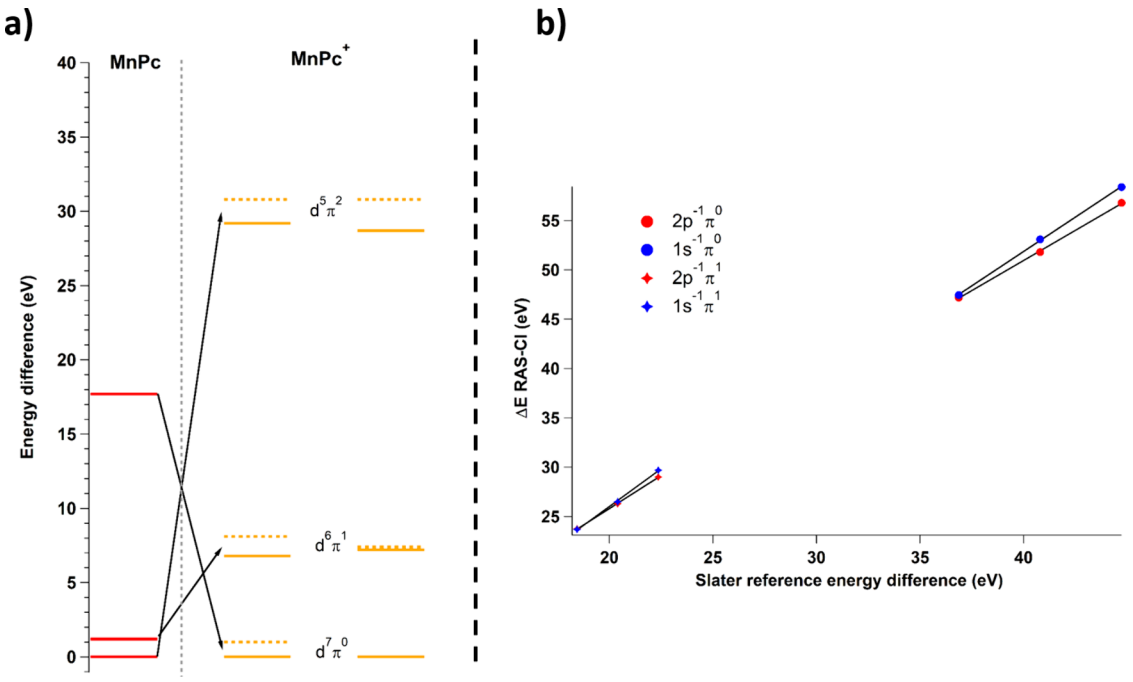

Figure 3. (a) Energy levels of $d^n\pi^m$ configurations examplified for MnPc. The ground state energy levels are colored dark red, while the corresponding ionic core hole states are colored orange. Ground and ionic states within MnPc are separated by a gray vertical dashed line. Arrows indicate the energy changes for the same valence configuration upon core ionization. Dashed horizontal lines correspond to electronic states with the lowest multiplicity, i.e., $2S + 1 = 3$. (b) ΔE (RAS-CI) energies for the $2p^{-1}$ and $1s^{-1}$ core-ionized states of each of the three MPc molecules plotted as a function of the Slater reference energy difference, both in electronvolts (see details on the model in the text). The red (blue) diamonds represent the $2p^{-1}\pi^1$ ($1s^{-1}\pi^1$) configuration energies, while red (blue) dots represent the $2p^{-1}\pi^0$ ($1s^{-1}\pi^0$) configuration energies for MnPc, FePc, and CoPc in increasing energy order.

considered between this state and all accessible $2p^{-1}$ single- and double-excitation configurations.

All calculations were performed using the quantum chemical software ORCA, version 5.0.3.[18,19] Spin−orbit coupling (SOC) effects were included using the spin−orbit mean field (SOMF) Hamiltonian[20−22] within an effective one-electron operator framework.[23]

Prior to the CASSCF/RAS-CI calculations, molecular geometries were optimized at the density functional theory (DFT) level using the hybrid Becke three-parameter Lee−Yang−Parr (B3LYP) functional in conjunction with the correlation-consistent polarized triple-ζ (cc-pVTZ) basis set.[24−26] These DFT calculations were used exclusively to obtain equilibrium geometries. For the subsequent CASSCF/RAS-CI calculations, the cc-pwCVTZ basis set was employed for the metal center to account for core−valence correlation effects, while the cc-pVTZ basis set was used for all other atoms. The active spaces and the number of configurations included for each MPc molecule are detailed in the Supporting Information.

Finally, to facilitate comparison with experiment, the discrete transition intensities obtained were convoluted with a Gaussian function of 1.5 eV full width at half-maximum (fwhm) and with Lorentzian line widths of 0.6 eV for the $2p_{1/2}$ edge and 0.54 eV for the $2p_{3/2}$ edge. These values were found to provide the best agreement with the thick film experimental data reported by Bidermane et al.,[27] as shown in the Supporting Information. The present gas-phase spectra are affected by additional thermal broadening, which is discussed in the Supporting Information, where we also include a comparison between our simulations and the experimental data of Bidermane et al. (reprinted with permission) to further assess the quantitative level of agreement.

The experimental and simulated spectra of the MPc molecules are displayed in the top and bottom parts of Figure 2, respectively. MnPc is a $3d^5$ molecule generally accepted to have quartet character in its fundamental electronic state. However, its electronic configuration remains controversial, although two leading configurations are favored in the literature, namely, $b_{2g}^2e_g^2a_{1g}^1b_{1g}^0$ and $b_{2g}^1e_g^3a_{1g}^1b_{1g}^0$.[28−30] The present CASSCF calculation results in the $b_{2g}^1e_g^3a_{1g}^1b_{1g}^0$ electron configuration for the ground state. However, as stated in our previous study on FePc,[5] one has to be very cautious in drawing conclusions about the ground state configuration of such molecules since they would require a comprehensive study using spectra from different thresholds and theoretical methods, which is beyond the scope of this work. The experimental spectrum in Figure 2a displays two maxima at 646.8 and 658.5 eV, which correspond to the $2p_{3/2}^{-1}$ and $2p_{1/2}^{-1}$ states, respectively. In addition, each peak exhibits a tail on the high-energy side, which corresponds to unresolved satellites and shake-off final states that are not taken into account in the present calculation.[31] The overall agreement with theory is satisfactory. In particular, the shape and intensity ratio of the two main components are well reproduced by the calculations. However, the theoretical spin−orbit splitting is at 10.5 eV slightly smaller than the experimental value of 11.8 eV. Such a difference of ≈9% is also found for the other molecules and is typical for the SOMF approximation.

FePc (Figure 2b) is a $3d^6$ molecule with ground state $b_{2g}^2e_g^3a_{1g}^1b_{1g}^0(^3E_g)$.[5] The two main bands are due to the SOC of ≅13.5 eV, which is slightly larger than the present theoretical value of 12.3 eV.

https://doi.org/10.1021/acs.jpclett.6c00486
J. Phys. Chem. Lett. 2026, 17, 4804−4810

CoPc is a $3d^7$ molecule with electronic ground state $b_{2g}^2 e_g^4 a_{1g}^1 b_{1g}^0 ({}^2A_{1g})$ as obtained by the present CASSCF calculations in full agreement with the joint experimental and theoretical study combining DFT and CTM calculations.[32] In the experimental spectrum displayed in Figure 2c, the $2p_{3/2}$ component is located at ≈786.0 eV and the $2p_{1/2}$ one at ≈801.8 eV; i.e., the energy difference is larger than the calculated value of 14.4 eV. Furthermore, there is a pronounced shoulder at a binding energy of ≈788.5 eV. Although this shoulder is partially masked by the present experimental resolution, it is clearly visible in spectra recorded for films (see, for example, the work of Uihlein et al.[33]). This spectral feature is reproduced by the present calculations and assigned to a mixed configuration from $S = 3$ and $S = 1$ spin states.

Note that the theoretical spectra are shifted by −3, −2.9, and −0.9 eV for MnPc, FePc, and CoPc, respectively, to match the experimental data. These small deviations ($<5 \times 10^{-3}$ in relative energy) do not correspond to the calculated absolute binding energies for the $2p^{-1}$ electronic states, but to the difference between the $1s^{-1}$ and $2p^{-1}$ states. Note that the absolute binding energies in the RAS-CI calculations are overestimated by ≈30 eV.

To gain insight into the electronic configurations at play in the photoelectron spectra, we analyzed the relative energies of the leading contributions given by the RAS-CI calculation. The energy differences for the various spin and occupation patterns in the neutral and core-ionized states are summarized in Table S4. Figure 3a shows the energy levels for MnPc as compared to the global minimum of each manifold, i.e., the ground state (dark red) and $2p^{-1}$ and $1s^{-1}$ core-ionized states (lighter colors). The smallest multiplicities $2S + 1$ of the core hole states are indicated by dashed horizontal lines. Since the effects are strikingly similar for all studied MPc molecules, we show the results for only MnPc. Interestingly, we observe a drastic rearrangement of the energy levels between the ground- and core-ionized state. Across all three systems, we observe a systematic stabilization of configurations involving a double ligand-to-metal charge transfer ($\pi \rightarrow 3d$) upon core ionization, with comparable magnitudes of approximately 30 eV.

These trends are particularly striking, because the RAS-CI computations were performed without any explicit orbital relaxation of the core-ionized states. The observed stabilization originates, therefore, from the electrostatic $(Z + 1)$ screening effect of the core hole, captured through electronic correlation and configuration interaction rather than from variational orbital shape changes.

In the ground state, the preference for a doubly occupied π orbital rather than an additional population of empty 3d orbitals leading to neutral metal atoms arises from two well-known effects. (i) The $3d_{x^2-y^2}(b_{1g})$ orbital lies particularly high in energy due to its strong antibonding interaction with the nitrogen lone pairs of the macrocycle, and (ii) the strong ligand field generated by the phthalocyanine increases the energy of the remaining 3d orbitals, leading to a high-spin configuration without further 3d filling.

Upon creation of a localized core hole ($1s^{-1}$ or $2p^{-1}$), the situation reverses. The 3d orbitals experience an effective $Z + 1$ potential as the screening decreases strongly and they are stabilized. This effect can be quantified by a simple $Z + 1$/Slater model.[34] For a 3d electron, the orbital energy can be approximated by

$$E_{3d} \approx -\frac{Z_{eff}^{\ 2}}{n^2} R_y \ (n = 3,\ R_y = 13.61\text{eV}) \tag{3}$$

so that a change ΔZ_{eff} in effective nuclear charge Z_{eff} results in an energy shift

$$\Delta E_{3d} \approx -\frac{(2Z_{eff}\Delta Z_{eff} + \Delta Z_{eff}^{\ 2})}{n^2} R_y \tag{4}$$

Using Slater's rules,[34] a 3d electron in Mn, Fe, or Co sees in the electronic ground state an effective charge Z_{eff} of ≈5.5−7.0. Creating a 2p or 1s hole effectively increases Z_{eff} by ≈1, leading to a ΔE_{3d} of approximately −18 to −22 eV per 3d electron. Two $\pi \rightarrow$ 3d charge-transfer processes therefore yield an electrostatic stabilization on the order of 35−45 eV. Accounting for the energetic cost of depopulating two π electrons as well as additional relaxation effects reduces this value to a net stabilization of about 30 eV, in good agreement with the RAS-CI results.

This analysis shows that the large stabilization of $\pi^0 3d^{n+2}$ configurations in the core-ionized states originates from a purely electronic screening response to core hole perturbation. In other words, the core hole acts as a local "$Z + 1$" field that reorganizes the 3d−π energy balance through Coulombic effects alone.

To rationalize the magnitude of the energy stabilization observed at both ionization thresholds, we compared the RAS-CI values with the prediction of the simple electrostatic model based on Slater's rules. This comparison (see Figure 3b and Table S6) reveals a linear correlation for all MPc molecules, at the 2p and 1s levels. The slopes, ranging between 1.2 and 1.5, indicate a systematic scaling between the *ab initio* and atomic-like descriptions. This linearity suggests that (i) the observed stabilization upon core ionization follows a general trend across metallophthalocyanines, (ii) it could be extended to other transition-metal complexes upon accumulation of extensive data sets, and (iii) it provides a straightforward way to estimate RAS-CI core hole binding energies from an analytical evaluation of the Slater-type stabilization energy.

In conclusion, we have combined experiment and multi-configurational *ab initio* simulations to investigate the impact of metal 2p core ionization on the electronic structure of metallophthalocyanines. For MnPc, FePc, and CoPc, the calculated X-ray photoelectron spectra show nearly quantitative agreement with experiment. In all three cases, we also reveal a robust and unexpected electronic response to core ionization. In all three systems, the neutral $\pi^2 d^n$ valence configuration is destabilized upon creation of a 2p core hole, while doubly excited ligand-to-metal charge-transfer configurations ($\pi^0 d^{n+2}$) become energetically favored in the final state manifold.

Beyond this qualitative picture, we identify across different metals and ionization thresholds an almost linear correlation with slopes ranging from 1.2 to 1.5 between the stabilization energies obtained from RAS-CI calculations and a simple hydrogenic/Slater screening estimate. This correlation highlights the dominant role of Coulombic screening in the electronic response to core ionization. It also provides an intuitive and metal-dependent parameter to estimate whether single or double charge-transfer final states are expected to dominate and to estimate their energetic separation prior to explicit configuration interaction calculations.

The present study also highlights the scope and limitations of the approach. When satellite intensities are high, as in the

https://doi.org/10.1021/acs.jpclett.6c00486
J. Phys. Chem. Lett. 2026, 17, 4804−4810

case of CuPc,[35] a single-reference description of the $1s^{-1}$ intermediate state is insufficient to reproduce the experimental spectra. Similarly, single-reference descriptions of MPc 3p photoelectron spectra are not quantitative due to the strong 3p−3d correlation and ligand field splitting. Addressing these cases will require extensions beyond the present framework, such as multireference descriptions of the core-ionized state, state-specific orbital optimization, and/or the inclusion of perturbative dynamical correlation.

Overall, these results demonstrate that metal 2p core ionization can fundamentally reshape the valence electronic structure of transition-metal complexes. By combining quantitative spectroscopy with a transparent electrostatic interpretation and a transferable scaling relation, this work provides both physical insight and predictive guidance for the analysis of core-level spectra and opens the way to broader applications beyond metallophthalocyanines.

■ ASSOCIATED CONTENT

Supporting Information

The Supporting Information is available free of charge at https://pubs.acs.org/doi/10.1021/acs.jpclett.6c00486.

(i) Derivation of the intensities for X-ray photoelectron and X-ray emission spectra, (ii) the xyz coordinates of the MPc molecules, (iii) A discussion on the thermal broadening, (iv) description of the active spaces used for the CASSCF/RASCI calculations, (v) detailed ORCA inputs for the CASSCF and RASCI calculations, (vi) description of the optimized orbitals and found energy levels, and (vii) a discussion on the comparison of the Slater's model and our RASCI calculations (PDF)

■ AUTHOR INFORMATION

Corresponding Author

G. Goldsztejn − *Université Paris-Saclay, Institut des Sciences Moléculaires d'Orsay ISMO, UMR CNRS 8214, F-91405 Orsay, France;* orcid.org/0000-0002-9123-6419; Email: gildas.goldsztejn@cnrs.fr

Authors

S. Carniato − *Sorbonne Université, CNRS, Laboratoire de Chimie Physique - Matière et Rayonnement, LCPMR, 75005 Paris, France;* orcid.org/0000-0001-6292-4688

R. Püttner − *Freie Universität Berlin, Berlin D-14195, Germany*

M. Briant − *Univ. Paris-Saclay, CEA, CNRS, NIMBE (UMR 3685), 91191 Gif-Sur-Yvette, France*

E. Gloaguen − *Université Paris-Saclay, Institut des Sciences Moléculaires d'Orsay ISMO, UMR CNRS 8214, F-91405 Orsay, France;* orcid.org/0000-0002-1023-2791

K. Marmorat − *Université Paris-Saclay, Institut des Sciences Moléculaires d'Orsay ISMO, UMR CNRS 8214, F-91405 Orsay, France;* orcid.org/0009-0008-5797-6705

M. Labeye − *Laboratory CPCV, Department of Chemistry, École Normale Supérieure, PSL University, Sorbonne Université, CNRS, 75005 Paris, France;* orcid.org/0000-0002-8838-2626

P. Çarçabal − *Univ Toulouse, CNRS, Laboratoire Collisions Agrégats Réactivité, 31400 Toulouse, France;* orcid.org/0000-0002-4738-115X

Complete contact information is available at: https://pubs.acs.org/10.1021/acs.jpclett.6c00486

Notes

The authors declare no competing financial interest.

■ REFERENCES

(1) Walzer, K.; Maennig, B.; Pfeiffer, M.; Leo, K. Highly efficient organic devices based on electrically doped transport layers. *Chem. Rev.* **2007**, *107*, 1233−127.

(2) Domingo, N.; Bellido, E.; Ruiz-Molina, D. Advances on structuring, integration and magnetic characterization of molecular nanomagnets on surfaces and devices. *Chem. Soc. Rev.* **2012**, *41*, 258−302.

(3) Leznoff, C. C.; Lever, A. B. P. *Phthalocyanines, Properties and Applications*; VCH: New York, 1989.

(4) Reddi, E.; Lo Castro, G.; Biolo, R.; Jori, G. Pharmacokinetic studies with zinc(II)-phthalocyanine in tumour-bearing mice. *Br. J. Cancer* **1987**, *56*, 597−600.

(5) Laurent, J.; Bozek, J.; Briant, M.; Çarçabal, P.; Cubaynes, D.; Milosavljević, A.; Püttner, R.; Shafizadeh, N.; Simon, M.; Soep, B.; et al. Consistent characterization of the electronic ground state of iron(ii) phthalocyanine from valence and core-shell electron spectroscopy. *Phys. Chem. Chem. Phys.* **2022**, *24*, 2656−2663.

(6) Thole, B. T.; Van Der Laan, G.; Butler, P. H. Spin-mixed ground state of Fe phthalocyanine and the temperature-dependent branching ratio in X-ray absorption spectroscopy. *Chem. Phys. Lett.* **1988**, *149*, 295−299.

(7) Boydas, E.; Roemelt, M. The trials and triumphs of modelling X-ray absorption spectra of transition metal phthalocyanines. *Phys. Chem. Chem. Phys.* **2024**, *26*, 20376.

(8) Zhang, W.; Shu, C.; Zhan, J.; Zhang, S.; Zhang, L.-H.; Yu, F. Deep Electronic State Regulation through Unidirectional Cascade Electron Transfer Induced by Dual Junction Boosting Electrocatalysis Performance. *Adv. Sci.* **2023**, *10*, e2304063.

(9) Karstens, R.; Glaser, M.; Belser, A.; Balle, D.; Polek, M.; Ovsyannikov, R.; Giangrisostomi, E.; Chassé, T.; Peisert, H. FePc and $FePcF_{16}$ on Rutile TiO_2(110) and (100): Influence of the Substrate Preparation on the Interaction Strength. *Molecules* **2019**, *24*, 4579.

(10) Siritanaratkul, B.; Sharma, P. K.; Yu, E.; Cowan, A. Improving the Stability, Selectivity, and Cell Voltage of a Bipolar Membrane Zero-Gap Electrolyzer for Low-Loss CO 2 Reduction. *Adv. Mater. Interfaces* **2023**, *10*, 2300203.

(11) Glaser, M.; Peisert, H.; Adler, H.; Aygül, U.; Ivanovic, M.; Nagel, P.; Merz, M.; Schuppler, S.; Chassé, T. Electronic structure at transition metal phthalocyanine-transition metal oxide interfaces: Cobalt phthalocyanine on epitaxial MnO films. *J. Chem. Phys.* **2015**, *142*, 101918.

(12) Uihlein, J.; Peisert, H.; Glaser, M.; Polek, M.; Adler, H.; Petraki, F.; Ovsyannikov, R.; Bauer, M.; Chassé, T. Communication: Influence of graphene interlayers on the interaction between cobalt phthalocyanine and Ni(111). *J. Chem. Phys.* **2013**, *138*, 081101.

(13) Hocking, R. K.; Wasinger, E. C.; Yan, Y.-L.; deGroot, F. M. F.; Walker, F. A.; Hodgson, K. O.; Hedman, B.; Solomon, E. I. Fe L-Edge X-ray Absorption Spectroscopy of Low-Spin Heme Relative to Non-heme Fe Complexes: Delocalization of Fe d-Electrons into the Porphyrin Ligand. *J. Am. Chem. Soc.* **2007**, *129*, 113−125.

(14) Ryland, E. S.; Lin, M.-F.; Verkamp, M. A.; Zhang, K.; Benke, K.; Carlson, M.; Vura-Weis, J. Tabletop Femtosecond M-edge X-ray Absorption Near-Edge Structure of FeTPPCl: Metalloporphyrin Photophysics from the Perspective of the Metal. *J. Am. Chem. Soc.* **2018**, *140*, 4691−4696.

(15) Mosaferi, M.; Selles, P.; Miteva, T.; Ferté, A.; Carniato, S. Interpretation of Shakeup Mechanisms in Copper L-Shell Photoelectron Spectra. *J. Phys. Chem. A* **2022**, *126*, 4902−4914.

(16) Schmidt, V. *Electron Spectrometry of Atoms using Synchrotron Radiation*; Cambridge Monographs on Atomic, Molecular and Chemical Physics; Cambridge University Press, 1997.

(17) Pollock, C. J.; Delgado-Jaime, M. U.; Atanasov, M.; Neese, F.; DeBeer, S. Kβ Mainline X-ray Emission Spectroscopy as an Experimental Probe of Metal-Ligand Covalency. *J. Am. Chem. Soc.* **2014**, *136*, 9453−9463.
(18) Neese, F. The ORCA program system. *Wiley Interdiscip. Rev.: Comput. Mol. Sci.* **2012**, *2*, 73−78.
(19) Neese, F. Software update: the ORCA program system - Version 5.0. *Wiley Interdiscip. Rev.: Comput. Mol. Sci.* **2022**, *12*, e1606.
(20) Hess, B. A.; Marian, C. M.; Wahlgren, U.; Gropen, O. A mean-field spin-orbit method applicable to correlated wavefunctions. *Chem. Phys. Lett.* **1996**, *251*, 365−371.
(21) Schimmelpfennig, B. *AMFI, an atomic mean-field spin-orbit integral program*; University of Stockholm: Stockholm, 1996.
(22) Berning, A.; Schweizer, M.; Werner, H.-J.; Knowles, P. J.; Palmieri, P. Spin-orbit matrix elements for internally contracted multireference configuration interaction wavefunctions. *Mol. Phys.* **2000**, *98*, 1823−1833.
(23) Neese, F. Efficient and accurate approximations to the molecular spin-orbit coupling operator and their use in molecular -tensor calculations. *J. Chem. Phys.* **2005**, *122*, 034107.
(24) Prascher, B. P.; Woon, D. E.; Peterson, K. A.; Dunning, T. H.; Wilson, A. K. Gaussian basis sets for use in correlated molecular calculations. VII. Valence, core-valence, and scalar relativistic basis sets for Li, Be, Na, and Mg. *Theor. Chem. Acc.* **2011**, *128*, 69−82.
(25) Balabanov, N. B.; Peterson, K. A. Systematically convergent basis sets for transition metals. I. All-electron correlation consistent basis sets for the 3d elements Sc-Zn. *J. Chem. Phys.* **2005**, *123*, 064107.
(26) Balabanov, N. B.; Peterson, K. A. Basis set limit electronic excitation energies, ionization potentials, and electron affinities for the 3d transition metal atoms: Coupled cluster and multireference methods. *J. Chem. Phys.* **2006**, *125*, 074110.
(27) Bidermane, I.; Lüder, J.; Totani, R.; Grazioli, C.; de Simone, M.; Coreno, M.; Kivimäki, A.; Åhlund, J.; Lozzi, L.; Brena, B.; et al. Characterization of gas phase iron phthalocyanine with X-ray photoelectron and absorption spectroscopies. *Phys. Status Solidi B* **2015**, *252*, 1259−1265.
(28) Stepanow, S.; Lodi Rizzini, A.; Krull, C.; Kavich, J.; Cezar, J. C.; Yakhou-Harris, F.; Sheverdyaeva, P. M.; Moras, P.; Carbone, C.; Ceballos, G.; Mugarza, A.; Gambardella, P. Spin Tuning of Electron-Doped Metal-Phthalocyanine Layers. *J. Am. Chem. Soc.* **2014**, *136*, 5451−5459.
(29) Kroll, T.; Kraus, R.; Schönfelder, R.; Aristov, V. Y.; Molodtsova, O. V.; Hoffmann, P.; Knupfer, M. Transition metal phthalocyanines: Insight into the electronic structure from soft x-ray spectroscopy. *J. Chem. Phys.* **2012**, *137*, 054306.
(30) Brumboiu, I. E.; Totani, R.; de Simone, M.; Coreno, M.; Grazioli, C.; Lozzi, L.; Herper, H. C.; Sanyal, B.; Eriksson, O.; Puglia, C.; et al. Elucidating the 3d Electronic Configuration in Manganese Phthalocyanine. *J. Phys. Chem. A* **2014**, *118*, 927−932.
(31) Püttner, R.; Goldsztejn, G.; Céolin, D.; Rueff, J.-P.; Moreno, T.; Kushawaha, R. K.; Marchenko, T.; Guillemin, R.; Journel, L.; Lindle, D. W.; et al. Direct Observation of Double-Core-Hole Shake-Up States in Photoemission. *Phys. Rev. Lett.* **2015**, *114*, 093001.
(32) Zhang, T.; Brumboiu, I. E.; Lanzilotto, V.; Lüder, J.; Grazioli, C.; Giangrisostomi, E.; Ovsyannikov, R.; Sassa, Y.; Bidermane, I.; Stupar, M.; et al. Conclusively Addressing the CoPc Electronic Structure: A Joint Gas-Phase and Solid-State Photoemission and Absorption Spectroscopy Study. *J. Phys. Chem. C* **2017**, *121*, 26372−26378.
(33) Uihlein, J.; Polek, M.; Glaser, M.; Adler, H.; Ovsyannikov, R.; Bauer, M.; Ivanovic, M.; Preobrajenski, A. B.; Generalov, A. V.; Chassé, T.; et al. Influence of Graphene on Charge Transfer between CoPc and Metals: The Role of Graphene-Substrate Coupling. *J. Phys. Chem. C* **2015**, *119*, 15240−15247.
(34) Slater, J. C. Atomic Shielding Constants. *Phys. Rev.* **1930**, *36*, 57−64.
(35) Carniato, S.; Goldsztejn, G.; Benbalagh, R. Spectrum of copper phthalocyanine: An experimental and theoretical study. Manuscript in preparation, 2026.

NOTE ADDED AFTER ASAP PUBLICATION

Due to a production error, the version of this paper that was published ASAP April 8, 2026, contained a spelling error in the name of author P. Çarçabal. The corrected version posted April 8, 2026.

https://doi.org/10.1021/acs.jpclett.6c00486
J. Phys. Chem. Lett. 2026, 17, 4804−4810